nature materials

LETTERS

PUBLISHED ONLINE: 12 OCTOBER 2014 | DOI: 10.1038/NMAT4105

Liquid-like pseudoelasticity of sub-10-nm crystalline silver particles

Jun Sun[1†], Longbing He[1†], Yu-Chieh Lo[2,3,4†], Tao Xu[1], Hengchang Bi[1], Litao Sun[1*], Ze Zhang[5*], Scott X. Mao[6] and Ju Li[2,3*]

In nanotechnology, small-volume metals with large surface area are used as electrodes, catalysts, interconnects and antennae[1–4]. Their shape stability at room temperature has, however, been questioned. Using *in situ* high-resolution transmission electron microscopy, we find that Ag nanoparticles can be deformed like a liquid droplet but remain highly crystalline in the interior, with no sign of dislocation activity during deformation[5,6]. Surface-diffusion-mediated pseudoelastic deformation is evident at room temperature, which can be driven by either an external force or capillary-energy minimization. Atomistic simulations confirm that such highly unusual Coble pseudoelasticity can indeed happen for sub-10-nm Ag particles at room temperature and at timescales from seconds to months.

Nanotechnology requires precise shape control of components. Once a certain shape is made, it is often hoped that it stays unchanged over a long period of time. Nanoelectronic devices with 14 nm feature sizes are commercially available at present, and we may soon enter the sub-10-nm regime. It is therefore essential to examine the shape change and shape stability of sub-10-nm material components, especially close to room temperature.

Although both plastic and pseudoelastic deformations are used for shaping, and both incur energy dissipation, the essential difference is that, when unloaded to zero stress, a pseudoelastic component always recovers to a single 'rest shape' regardless of previous deformation history, whereas a component deformed by plasticity has no memory of a single rest shape and will stay in the deformed shape(s) at zero stress (see Supplementary Part 15 for an illustration of this difference). In this paper we will show using *in situ* high-resolution transmission electron microscopy that sub-10-nm single crystals of Ag deform pseudoelastically, rather than plastically, at room temperature. This victory of pseudoelasticity over plasticity at the small extremes of size-dependent mechanical behaviour of metals[5–9] can have three profound practical consequences: there is no longer 'plastic freedom' at the small extremes—that is, the availability of a large number of arbitrary, stress-free shapes; one can still gain access to an infinite number of shapes, but different finite loads must be imposed via external constraints, similar to inflating a rubbery balloon; omni-directional, reconfigurable and damage-tolerant contact is suddenly possible at this extreme scale.

Liquid-like deformation of silver nanocrystals

Figure 1 shows a typical cycle of compression and stretching of a silver (Ag) nanocrystal (NC) with a base diameter of 9.8 nm and partially bonded on the surface of a W tip. The NC height is 4.6 nm and the shape is stable under electron-beam irradiation during normal imaging (the beam intensity of 3.8 A cm^{-2} is much weaker than in normal practice)[10,11] (Methods and Supplementary Part 1). This shape probably possesses the minimum free energy. The facet shown in Fig. 1a corresponds to the (111) crystal plane of Ag (Supplementary Part 2). As the NC-decorated W tip approaches the crystalline ZrO_2 above (Fig. 1b), the top of the Ag NC snaps slightly onto the ZrO_2 surface, as a result of van der Waals attraction[12]. The upper part of the Ag NC is then deformed, as can be seen in Fig. 1c. As the W tip further approaches the ZrO_2, compressive stress is spread onto the entire Ag NC. In Fig. 1d–f, the Ag NC undergoes drastic deformation, resulting eventually in a flat pancake-like shape. During the process, the outer morphology of the Ag NC changes similarly to a liquid drop (Supplementary Movies 1–3). However, high-resolution images taken during the process prove that the deforming Ag nanoparticle remains single crystalline (Fig. 1k,l) inside. When the W tip is detached from the ZrO_2 (Fig. 1f–i), the Ag NC surprisingly starts to recover its original shape and the base diameter decreases from 14.3 to 9.5 nm in the first stage, and then to 9.2 nm. The height of the Ag NC recovered quickly and a thin sharp Ag tip meniscus (Fig. 1i) is formed. When the tip is finally detached, the shape of the Ag NC changes rapidly from an elongated spire to a stable geometry with facets similar to its initial ones (Fig. 1j). Such a reversible change in shape (except for missing atoms induced by effects such as tip scratching and electron bombardment, which break the ideal behaviour) is infinitely repeatable (Fig. 1m,n and Supplementary Movies 1 and 2) just like the deformation of a water droplet, also for lateral squeezing (Supplementary Part 16) and for smaller Ag NCs (Supplementary Movie 4). Thus, the videotaped deformations are pseudoelastic rather than plastic; the memory of a single rest shape can be explained by capillary-energy minimization—that is, the rest shape is the result of the balance between Ag surface energy and Ag–W interfacial energy.

Surface-diffusion-dominated Coble pseudoelasticity

Next we demonstrate that the atomic mechanism behind the shape evolution is surface diffusion. There is prior evidence in the

[1]SEU-FEI Nano-Pico Center, Key Lab of MEMS of Ministry of Education, Southeast University, Nanjing, 210096, China, [2]Department of Nuclear Science and Engineering, Massachusetts Institute of Technology, Cambridge, Massachusetts 02139, USA, [3]Department of Materials Science and Engineering, Massachusetts Institute of Technology, Cambridge, Massachusetts 02139, USA, [4]Center for Elements Strategy Initiative for Structural Materials (ESISM), Kyoto University, Sakyo, Kyoto 606-8501, Japan, [5]Department of Materials Science and Engineering, State Key Laboratory of Silicon Materials, Zhejiang University, Hangzhou 310027, China, [6]Department of Mechanical Engineering and Materials Science, University of Pittsburgh, 3700 O'Hara Street, Pittsburgh, Pennsylvania 15261, USA. †These authors contributed equally to this work. *e-mail: slt@seu.edu.cn; zezhang@zju.edu.cn; liju@mit.edu

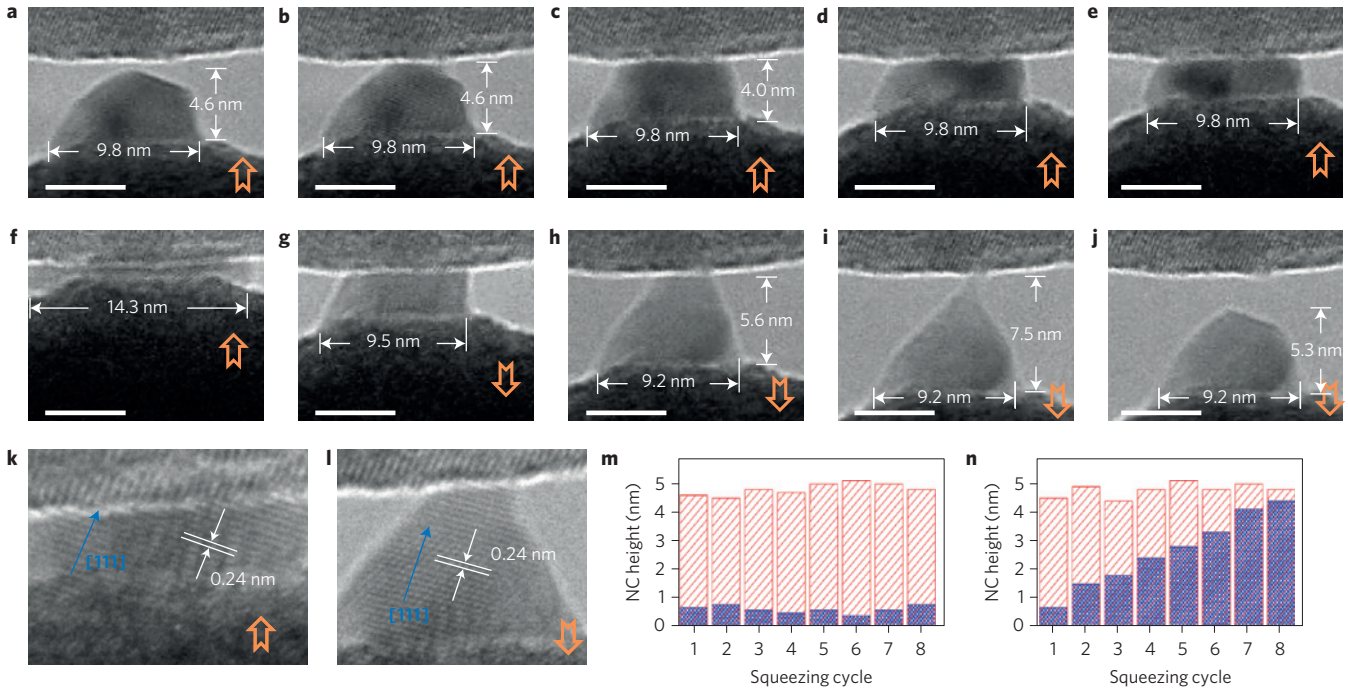

Figure 1 | Reversible pseudoelastic deformation of the Ag NC. a, Initial geometry of the Ag NC. The diameter of the base is 9.8 nm and the height is 4.6 nm. **b–i**, Dynamic shape evolution of the Ag NC during compression and stretching. The base part retained its size in the first stages of compression, and later turned to a pancake-like structure. During stretching, the base almost recovered its initial size, with a slight decrease from 9.8 nm to 9.2 nm. **j**, Final geometry of the Ag NC. **k**,**l**, A snapshot of the Ag NC during deformation. The lattice fringes indicate that the NC is crystalline. The crystal orientation is maintained during deformation (blue arrows). The orange arrows indicate the movement direction of the W tip. **m**,**n**, Repetitive compression of the Ag NC to the same (**m**) and different (**n**) heights for eight cycles. The NC height in each cycle was measured during (blue columns) and after (red columns) compression. All scale bars, 5 nm.

literature[5,6] of the dislocation-free diffusional deformation of gold. Here, the imposed stress could be relieved by atom plating/ablation from Ag surfaces to Ag–W or Ag–ZrO_2 interfaces, as in diffusive Coble creep[13], rather than by displacive dislocation slip, which is normally expected at room temperature[14]. This is evidenced by the direct high-resolution observation of another Ag NC. As shown in Fig. 2, a triangularly shaped Ag NC is compressed gently. Initially, the Ag NC presents a nearly stable geometry during imaging, apart from some flickering sites on the surface steps (Supplementary Movie 5), indicating that the atoms on those sites must be more active diffusively. When the W tip reaches the Ag NC, a fresh atomic layer is instantly formed, as marked by the black arrow in Fig. 2b. The new atomic layer grows along the surface when more compression is applied by the W tip (Fig. 2c,d), which clearly cannot be induced by a dislocation slip that would have caused a Burgers-vector-oriented surface step. When the W tip moves further, the whole Ag NC deforms, exhibiting a liquid-like change in morphology (Supplementary Movie 6), with continuous rather than discrete changes of morphology[14]. Simulation of this compression process (Fig. 2e) shows that the diffusion of atoms on free surfaces quickly reconstructs the geometry of the Ag NC, although the electron beam may accelerate this process slightly[15]. We define such deformation behaviour as 'Coble pseudoelasticity', meaning a liquid-like recoverable shape change while the atomic structure inside remains single crystalline. Coble pseudoelasticity has a similar physical origin to Coble creep, which can contribute to the room-temperature plasticity of nanocrystalline metals[16]. However, creep strain is expected to be fully plastic, whereas pseudoelastic strain is expected to be fully recoverable as the applied load returns to zero. Coble pseudoelasticity also differs from conventional pseudoelasticity in that it is not driven by martensitic transformations, but by surface diffusion.

We want to demonstrate that capillary energy plays a critical role in the memory and recall of the single rest shape in Coble pseudoelasticity. Thermodynamically, the surface energy is always there, as used in the Wulff construction (now also balanced by the interfacial energy). But to show that, kinetically, the surface energy is sufficient to drive the shape change of a sub-10-nm Ag NC at room temperature and timescales of seconds to months, a thin Ag nanowire is stretched to failure, forming a so-called mechanical break junction[17] such as that frequently used in molecular-electronics devices. We then observe the subsequent shape recovery at room temperature. As shown in Fig. 3, the diameter of the broken Ag tip is just a few nanometres. The initial size of the monitored area, as marked by the black stripes, is 10 nm in Fig. 3a. Immediately after the wire is fractured and the break junction forms, it shrinks rapidly in the first few seconds, as shown in Fig. 3a–d. The structure of the base part of the Ag tip remains unchanged, and dislocation activity is not observed[5,6]. However, the free surfaces on the upper part of the Ag tip undergo a continuous (not discrete) shape change, without any external stress, revealing significant capillary action at room temperature. The recession rate of the Ag tip is estimated to be $\sim$1 nm s^{-1} initially (Fig. 3a–c) and then decreases markedly (Supplementary Movie 7), agreeing with the theoretical prediction that the shrinking rate should scale as $\dot{h} \propto R^{-n}$, where R is the radius of curvature and n is a large exponent. According to classical curvature-driven surface diffusion theory, $n = 3$ (Supplementary Part 10). But kinetic Monte Carlo (kMC) simulations have revealed n to be as large as 15 at temperatures below the surface roughening transition[18], owing to facet nucleation controlled kinetics[18,19] not accounted for by continuous-curvature-driven surface-diffusion theory. Also, one can show that, when deforming under external mechanical stress σ, for fixed strain rate $\dot{\varepsilon}$ and temperature, the behaviour is $\sigma \propto R^n$, so 'smaller is very much

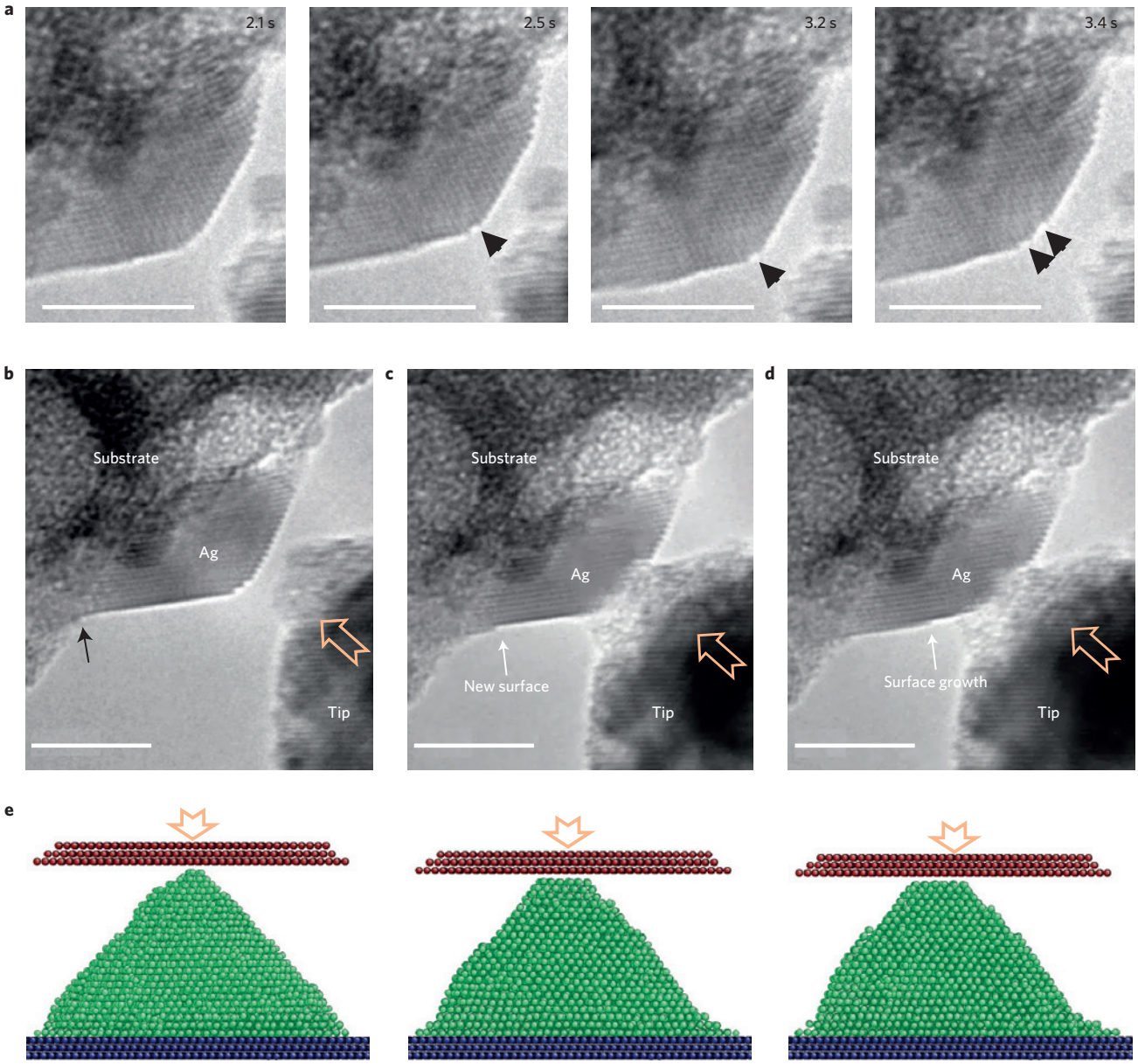

Figure 2 | Atomic layer growth during compression. a, Flickering atoms on free surface of the Ag NC (black arrowheads). See also Supplementary Movie 5. **b**, Initial geometry of a nanometre-sized Ag NC. **c**,**d**, Growth of a fresh atomic layer after gently applying a compressive load. See also Supplementary Movie 6. **e**, Simulated compression process of a Ag NC. The orange arrows indicate the movement direction of the tip. All scale bars, 5 nm.

weaker' in the Coble deformation regime. The crossover from the Hall–Petch-like 'smaller is stronger' trend $\sigma \propto R^{-\alpha}$ (α is usually between 0.5 and 1) when displacive plasticity is active to the 'smaller is very much weaker' diffusive Coble deformation regime $\sigma \propto R^{n}$ should be sharp and sudden as R is reduced, owing to the large positive exponent n. Put simply, we expect the strength to drop precipitously with reducing size in the very small extremes.

Coble pseudoelasticity confirmed by atomistic calculations

Inevitably, the imaging electron beam has some effects on the sample[20]. Although we do not expect it to alter the rest shape, electron-beam activation may accelerate surface diffusion (Supplementary Part 14). To ascertain whether Coble pseudoelasticity requires an electron beam to be feasible at room temperature, we perform atomistic calculations to simulate the shape relaxation of a Ag NC break junction (Supplementary Movies 8–10). Because of the limited accessible timescale of MD simulations, one strategy is to perform MD at higher temperatures, and then appropriately extrapolate to room temperature. The shape changes of MD simulations at 800 K for $t^{\mathrm{MD}}_{800\,\mathrm{K}} = 0.1\,\mu\mathrm{s}$ are found to be similar in magnitude and form (Fig. 3e–g) to the TEM observations. Detailed analysis of the atomic trajectories in the 800 K MD simulations (Supplementary Movie 8) show that: the shape evolution was dominated by single adatom movements, rather than chain or island processes; the shape change was indeed accomplished by atom ablation of the surface layers with greater curvature and by growth of the surface layers with smaller curvature, while atoms two monolayers below the surface always remained highly crystalline; the shape change is rate-controlled by atomic processes on non-(111) facets of the NC, as processes on (111) facets occurred much faster. These findings corroborate a database of activation-energy barriers (summarized in Supplementary Table 1) for FCC metal surface diffusion[21,22]. The ranking of the activation energy

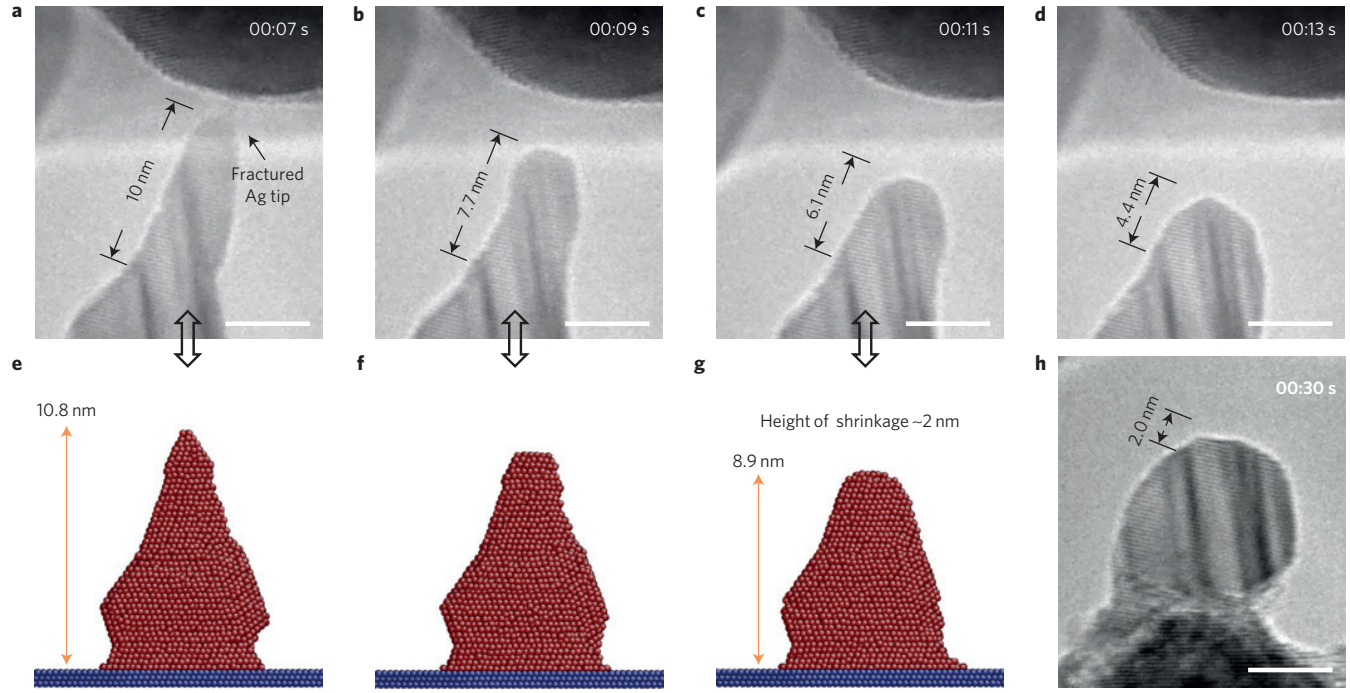

Figure 3 | Surface-energy-driven shape change. a, Initial geometry of the Ag tip after fracture. **b**–**d**, Shrinkage process of the Ag tip towards the base part after fracture. **e**–**g**, MD simulations showing that the shrinkage process of the Ag nanoparticle tip is consistent with the experiments in **a**–**c**. **h**, When the radius of curvature of the particle increased, the shrinkage process became slower. All scale bars, 5 nm.

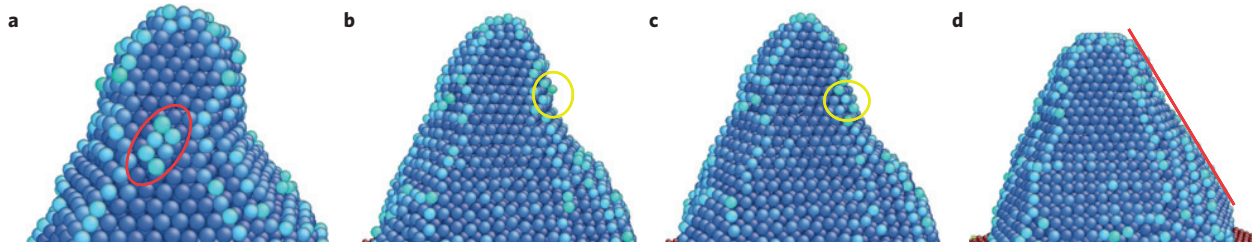

Figure 4 | Simulated shape evolution of Ag NCs by surface diffusion. a, Island diffusion (red circle) was observed only on (111) surfaces. **b**,**c**, The potholed surfaces were smoothed through a series of adatom migration and local reconstruction (yellow circles) on (001) facets. **d**, After a long time (0.1 μs), the sharp tip became blunter and the evolution slowed. 0.1 μs in the MD model at 800 K was long enough to mimic the shape change caused by Coble creep on the Ag NC at room temperature. The colour gradient represents the difference in potential energy per atom; dark blue represents lower energy and light blue represents higher energy.

barriers of single adatom hopping on different surface facets is: $(110)_{\text{out-channel}} > (001) > (110)_{\text{in-channel}} > (111)$. Atom-chain diffusion was also observed on (111) surfaces (Fig. 4a) and dispersed at the edges with other planes: chain processes were not found on the other facets[21]. The barriers against ascending adatoms are higher than those against descending adatoms, and the barriers for adatoms leaving a corner are higher than for those approaching a corner[22]—thus, high-curvature regions tend to be flattened, a manifestation of the Gibbs–Thomson effect on the chemical potential, which drives the pseudoelasticity. When adatoms arrived at uneven surfaces, they reordered the defective surface by a series of hopping, exchange or pyramid-collapse atomic events, as shown in Supplementary Movie 8 and Fig. 4d. The 'pothole-free' new surface then lowers the barriers for subsequent diffusing atoms[23–26] (Fig. 4b,c).

MD simulations also showed that the Ag NC surface mostly consisted of (111) and (001) facets, as well as defective sites near corners or terraces. Many adatoms and small clusters were found on the surface of those facets at the particle tip (Fig. 4). The crystallographic planes on the tip of 10 nm Ag nanoparticles coincide with the Wulff construction for Ag/Au (refs 27,28). We quantitatively estimated the timescale for room-temperature Coble pseudoelasticity, τ, by applying two newly developed accelerated MD simulation schemes[29,30] on (001) surface diffusion, which should be rate-controlling in the shape evolution. The distribution of average transition times at different temperatures shows a straight-line behaviour in the Arrhenius plot (Fig. 5). The timescale of diffusion events between 300 and 800 K shows only a small difference on (111), but varies by 5 ~ 6 decades for adatom diffusion on the (001) surface, owing to the larger activation energy. The enthalpy of a 10 nm Ag particle presents a linear relationship between 300 K and 800 K (Supplementary Fig. 4), which suggests no phase transformation in this temperature range. Therefore, most diffusion processes occurring at 800 K may be extrapolated to 300 K directly in the Arrhenius fashion. According to the data in Supplemetary Table II, we extrapolated the timescale of the shape change at 300 K by $t^{\text{MD}}_{800\,\text{K}}$ (MD simulation time at 800 K) $\times 10^{5\sim6}$ (difference of timescale). Thus, we conclude that the shape evolution or shape relaxation timescale at room temperature should be $\tau = 0.01 \sim 0.1$ s for the simulated geometry.

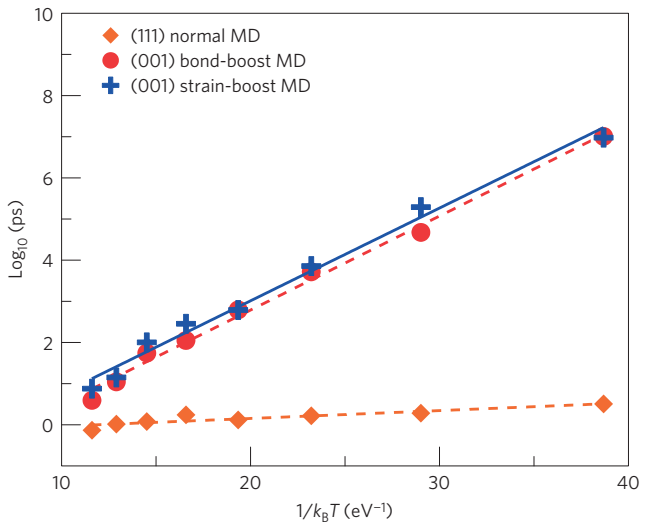

Figure 5 | Arrhenius plots of the transition time for diffusion events on the (001)/(111) surfaces of Ag NCs. Arrhenius plots of the transition time presented as a function of temperature for adatom-diffusion events on (001) and (111) surfaces. We used this Arrhenius relationship to extrapolate the timescale for the Ag-tip shrinkage process at room temperature.

Coble pseudoelasticity (rather than plasticity) is defined by a shape-relaxation time τ falling below anthropological observation timescales. Our MD and accelerated MD simulations indicate that, even in the absence of an electron beam, Coble pseudoelasticity should occur for sub-10-nm Ag crystals at room temperature. This is corroborated by the following. kMC simulations performed on a generic FCC noble metal showed that $\tau \sim 100$ s for a 1,728-atom nanocrystal[18] at $T = 300$ K (the parameters of the kMC simulation are not specifically for Ag). In a separate experiment, a nanogap was created between two ~20 nm Au tips, then left for four months, after which it was found that 'The nanogap has clearly expanded, and the locations of greatest curvature have been smoothed out'[31]. Given T_{melt} (Au) = 1,337 K > T_{melt} (Ag) = 1,235 K, sub-10-nm Ag tips should have τ much smaller than 20 nm Au tips. Based on power laws[18] and experimental data[31], one can then estimate an upper-bound of $\tau < 100$ s for sub-10-nm Ag tips, corroborating the basic conclusion of our simulations that τ falls near the convenient timeframe of seconds without electron-beam effects. Thus, surface diffusion indeed severely threatens the shape stability of sub-10-nm scale metallic interconnects at room temperature, even for metals with relatively high melting points such as Ag.

Conclusion

We want to emphasize that although the deformation behaviours are pseudoelastic and 'liquid-like', the nanoparticles have not melted, as the Ag NC remains highly crystalline, and both calculations and previous experimental work[5,6,32–36] have shown that the melting points of Ag, Au, Al, Cu and other metals at a size scale of 5 nm are still very much above room temperature. Thus, the phenomenon we observe is new and distinct from the well-known size-dependent melting point suppression effect[32]. What we see is deformation kinetics, not thermodynamic behaviour of the nanoparticles, and one can see this effect only when one tries to manipulate and follow the nanoparticles *in situ* (Supplementary Part 13).

In summary, the shape change of sub-10-nm Ag nanoparticles at room temperature is found to be dominated by surface diffusion, making them deform like liquid drops but with a highly crystalline core, which is fundamentally different from displacive shear plasticity by dislocations[14], and rather unexpected at such a low homologous temperature ($T/T_M = 0.24$). The triumph of pseudoelasticity over plasticity at the small extremes of size-dependent mechanical behaviour of metals can have profound practical consequences on the precise shaping and life estimation of nanometre-scale metallic contacts. It may also open a new avenue for shape-controlling nanodevices with finite forces; for example, the production of omni-directional, reconfigurable and damage-tolerant electrical contacts at room temperature, operated using relatively low forces.

Methods

Fabrication and characterization of Ag NCs. The Ag NCs were formed *in situ* on a ZrO_2 surface by electrically processing a microdevice with a TEM-scanning-tunnelling-microscope W probe (see Supplementary Fig. 1). The device had a sandwich-like micro-structure (ZrO_2–Ag–ZrO_2) and was prepared by gas-phase deposition. The structural evolution was characterized by TECNAI 20 TEM and aberration-corrected TEM (Titan 80–300) with video recorded at 10 frames s^{-1}. Compression and stretching cycles of the Ag NCs were conducted at a speed of approximately 0.1 nm s^{-1}. During forcible squeezing, the movement speed was approximately 1 nm s^{-1}.

MD and accelerated MD simulations. MD simulations were performed using the LAMMPS program[37]. The embedded-atom method (EAM) potential[38] was applied to describe the interactions between Ag atoms. A flat (111) plane indenter was used to compress and stretch the Ag particles. The interaction force between the indenter and particles was a Lennard-Jones potential with $\varepsilon = 0.18$ eV and $\sigma = 3.49$ A. After stretching, the sharp-tipped Ag particle was relaxed at 300, 800, 900, and 1,000 K, respectively, for 0.1 μs to observe the shape evolution. In the accelerated MD simulations, a six-layer slab with 72 atoms in each layer was established, and an adatom was put on the top of (001) surface. The two bottom layers were fixed and the others were mobile. Only the atoms in top two layers (including the adatom) were tagged for boosting by the strain-boost[29] and bond-boost[30] methods. The Nose–Hoover NVT ensemble was applied to both MD and accelerated MD. The transition time obtained from accelerated MD at each temperature was the average of ten samplings, which include hopping, exchanging and multiple exchanging events. The parameters of accelerated MD are 0.4 eV for the boost potential and 0.3 for the boost threshold[29]. Both values are chosen very conservatively after many tests.

Received 26 November 2013; accepted 4 September 2014; published online 12 October 2014

References

1. Park, M. *et al.* Highly stretchable electric circuits from a composite material of silver nanoparticles and elastomeric fibres. *Nature Nanotech.* **7,** 803–809 (2012).
2. Chen, J. Y., Lim, B., Lee, E. P. & Xia, Y. N. Shape-controlled synthesis of platinum nanocrystals for catalytic and electrocatalytic applications. *Nano Today* **4,** 81–95 (2009).
3. Liu, N., Tang, M. L., Hentschel, M., Giessen, H. & Alivisatos, A. P. Nanoantenna-enhanced gas sensing in a single tailored nanofocus. *Nature Mater.* **10,** 631–636 (2011).
4. Muhlschlegel, P., Eisler, H. J., Martin, O. J. F., Hecht, B. & Pohl, D. W. Resonant optical antennas. *Science* **308,** 1607–1609 (2005).
5. Rodrigues, V., Fuhrer, T. & Ugarte, D. Signature of atomic structure in the quantum conductance of gold nanowires. *Phys. Rev. Lett.* **85,** 4124–4127 (2000).
6. Rodrigues, V. & Ugarte, D. Real-time imaging of atomistic process in one-atom-thick metal junctions. *Phys. Rev. B* **63,** 073405 (2001).
7. Uchic, M. D., Dimiduk, D. M., Florando, J. N. & Nix, W. D. Sample dimensions influence strength and crystal plasticity. *Science* **305,** 986–989 (2004).
8. Yu, Q. *et al.* Strong crystal size effect on deformation twinning. *Nature* **463,** 335–338 (2010).
9. Brinckmann, S., Kim, J. Y. & Greer, J. R. Fundamental differences in mechanical behavior between two types of crystals at the nanoscale. *Phys. Rev. Lett.* **100,** 155502 (2008).
10. Iijima, S. & Ichihashi, T. Structural instability of ultrafine particles of metals. *Phys. Rev. Lett.* **56,** 616–619 (1986).
11. Wang, Z. W. & Palmer, R. E. Determination of the ground-state atomic structures of size-selected Au nanoclusters by electron-beam-induced transformation. *Phys. Rev. Lett.* **108,** 245502 (2012).
12. Mordehai, D., Rabkin, E. & Srolovitz, D. J. Pseudoelastic deformation during nanoscale adhesive contact formation. *Phys. Rev. Lett.* **107,** 096101 (2011).
13. Coble, R. L. A model for boundary diffusion controlled creep in polycrystalline materials. *J. Appl. Phys.* **34,** 1679–1682 (1963).
14. Zheng, H. *et al.* Discrete plasticity in sub-10-nm-sized gold crystals. *Nature Commun.* **1,** 144 (2010).

15. Wang, Z. W. & Palmer, R. E. Mass spectrometry and dynamics of gold adatoms observed on the surface of size-selected Au nanoclusters. *Nano Lett.* **12,** 91–95 (2012).
16. Gleiter, H. Nanocrystalline materials. *Prog. Mater. Sci.* **33,** 223–315 (1989).
17. Reed, M. A., Zhou, C., Muller, C. J., Burgin, T. P. & Tour, J. M. Conductance of a molecular junction. *Science* **278,** 252–254 (1997).
18. Combe, N., Jensen, P. & Pimpinelli, A. Changing shapes in the nanoworld. *Phys. Rev. Lett.* **85,** 110–113 (2000).
19. Mullins, W. W. & Rohrer, G. S. Nucleation barrier for volume-conserving shape changes of faceted crystals. *J. Am. Ceram. Soc.* **83,** 214–216 (2000).
20. Egerton, R. F., Li, P. & Malac, M. Radiation damage in the TEM and SEM. *Micron* **35,** 399–409 (2004).
21. Kim, S. Y., Lee, I. H. & Jun, S. Transition-pathway models of atomic diffusion on fcc metal surfaces. I. Flat surfaces. *Phys. Rev. B* **76,** 245407 (2007).
22. Kim, S. Y., Lee, I. H. & Jun, S. Transition-pathway models of atomic diffusion on fcc metal surfaces. II. Stepped surfaces. *Phys. Rev. B* **76,** 245408 (2007).
23. Aminpour, M., Trushin, O. & Rahman, T. S. Effect of misfit dislocation on surface diffusion. *Phys. Rev. B* **84,** 035455 (2011).
24. Ala-Nissila, T., Ferrando, R. & Ying, S. C. Collective and single particle diffusion on surfaces. *Adv. Phys.* **51,** 949–1078 (2002).
25. Yildirim, H., Kara, A. & Rahman, T. S. Origin of quasi-constant pre-exponential factors for adatom diffusion on Cu and Ag surfaces. *Phys. Rev. B* **76,** 165421 (2007).
26. Yildirim, H. & Rahman, T. S. Diffusion barriers for Ag and Cu adatoms on the terraces and step edges on Cu(100) and Ag(100): An *ab initio* study. *Phys. Rev. B* **80,** 235413 (2009).
27. Wang, B. Y., Liu, M. X., Wang, Y. T. & Chen, X. S. Structures and energetics of silver and gold nanoparticles. *J. Phys. Chem. C* **115,** 11374–11381 (2011).
28. Marks, L. D. Experimental studies of small-particle structrures. *Rep. Prog. Phys.* **57,** 603–649 (1994).
29. Hara, S. & Li, J. Adaptive strain-boost hyperdynamics simulations of stress-driven atomic processes. *Phys. Rev. B* **82,** 184114 (2010).
30. Miron, R. A. & Fichthorn, K. A. Accelerated molecular dynamics with the bond-boost method. *J. Chem. Phys.* **119,** 6210–6216 (2003).
31. Strachan, D. R. *et al.* Clean electromigrated nanogaps imaged by transmission electron microscopy. *Nano Lett.* **6,** 441–444 (2006).
32. Couchman, P. R. & Jesser, W. A. Thermodynamic theory of size dependence of melting temperature in metals. *Nature* **269,** 481–483 (1977).
33. Lai, S. L., Carlsson, J. R. A. & Allen, L. H. Melting point depression of Al clusters generated during the early stages of film growth: Nanocalorimetry measurements. *Appl. Phys. Lett.* **72,** 1098–1100 (1998).
34. Bachels, T., Guntherodt, H. J. & Schafer, R. Melting of isolated tin nanoparticles. *Phys. Rev. Lett.* **85,** 1250–1253 (2000).
35. Asoro, M. A., Damiano, J. & Ferreira, P. J. Size effects on the melting temperature of silver nanoparticles: *In-situ* TEM observations. *Microsc. Microanal.* **15,** 706–707 (2009).
36. Lu, H. M., Li, P. Y., Cao, Z. H. & Meng, X. K. Size-, shape-, and dimensionality-dependent melting temperatures of nanocrystals. *J. Phys. Chem. C* **113,** 7598–7602 (2009).
37. Plimpton, S. Fast parallel algorithms for short-range molecular dynamics. *J. Comput. Phys.* **117,** 1–19 (1995).
38. Sheng, H. W., Kramer, M. J., Cadien, A., Fujita, T. & Chen, M. W. Highly optimized embedded-atom-method potentials for fourteen fcc metals. *Phys. Rev. B* **83,** 134118 (2011).

Acknowledgements

This work was supported by the National Basic Research Program of China under grant Nos. 2011CB707601 and 2012CB619402, the National Natural Science Foundation of China under grant Nos. 61274114, 113279028, 51201032 and 51071044, the Key Grant Project of Chinese Ministry of Education under grant No. 311019, and the Natural Science Foundation of Jiangsu Province under grant Nos. BK2011592 and BK2012024. Y-C.L. thanks E. Bitzek (Friedrich-Alexander-Universität Erlangen-Nürnberg) and J. C. Huang (National Sun Yat-Sen University) for kind support. J.L. and Y-C.L. would like to acknowledge support from NSF DMR-1120901 and DMR-1240933. Computational time on the Extreme Science and Engineering Discovery Environment (XSEDE) under grants TG-DMR130038, TG-DMR140003 and TG-PHY140014 is gratefully acknowledged.

Author contributions

L.S., J.L. and Z.Z. proposed and supervised the project, J.S., L.H., T.X. and H.B. performed the experiments, and Y-C.L. performed the simulations. L.S., J.L., Z.Z. and S.X.M. analysed data and wrote the manuscript. All the authors participated in discussions of the research.

Additional information

Supplementary information is available in the online version of the paper. Reprints and permissions information is available online at www.nature.com/reprints. Correspondence and requests for materials should be addressed to L.S., Z.Z. or J.L.

Competing financial interests

The authors declare no competing financial interests.

nature materials

SUPPLEMENTARY INFORMATION

DOI: 10.1038/NMAT4105

Liquid-like pseudoelasticity of sub-10-nm crystalline silver particles

Jun Sun[1,*], Longbing He[1,*], Yu-Chieh Lo[2,5*], Tao Xu[1], Hengchang Bi[1], Litao Sun[1†], Ze Zhang[3†], Scott X. Mao[2,4], Ju Li[2†]

[1]*SEU-FEI Nano-Pico center, Key Lab of MEMS of Ministry of Education, Southeast University, Nanjing, 210096, China*

[2]*Department of Nuclear Science and Engineering and Department of Materials Science and Engineering, Massachusetts Institute of Technology, Cambridge, Massachusetts 02139, USA*

[3]*Department of Materials Science, State Key Lab of Si Materials, Zhejiang University, Hangzhou, Zhejiang, 310008, China*

[4]*Department of Mechanical Engineering and Materials Science, University of Pittsburgh, 3700 O'Hara Street, Pittsburgh, Pennsylvania 15261, USA*

[5]*Center for Elements Strategy Initiative for Structural Materials (ESISM), Kyoto University, Sakyo, Kyoto 606-8501, Japan*

***These authors contributed equally to this work.**

DOI: 10.1038/NMAT4105

†Correspondence and requests for materials should be addressed to L.S. (email: slt@seu.edu.cn), J.L. (email: liju@mit.edu) or Z.Z. (email: ezhang@zju.edu.cn).

1. Experimental setup

Figure S1 shows the experimental setup of the STM-TEM holder. The piezotube is three dimensional movable and the movement accuracy is 20 pm in X and Y direction and 2.5 pm in Z direction (toward the sample end).

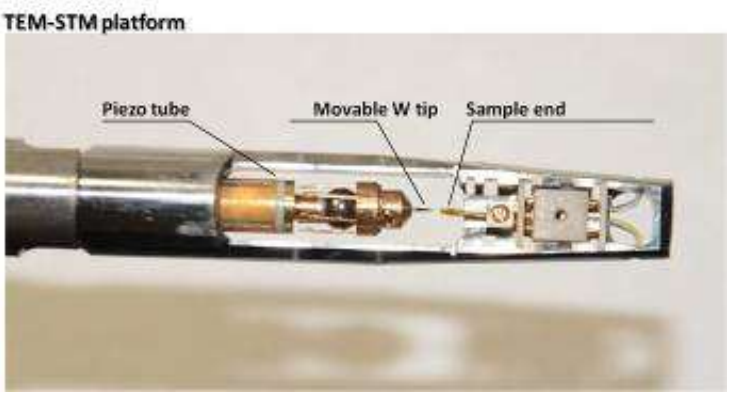

Figure S1| Experimental setup of STM-TEM holder. The sample is fixed onto the STM-TEM holder at one end, the counter end is a chemical-etched W tip fixed onto a movable piezotube.

2. Structure characterization of the Ag NCs

Figure S2 shows a high-resolution image of initial crystal structure of the Ag NC. The marked spot (0.24 nm) corresponds to the lattice spacing of (111) crystal plane. The hemisphere NC shows a featured geometry with a planar facet parallel to the (111) crystal plane on the top. The structure of the NC is stable and remains singe-crystalline. Figure S3 shows the crystal structure of the NC during compression.

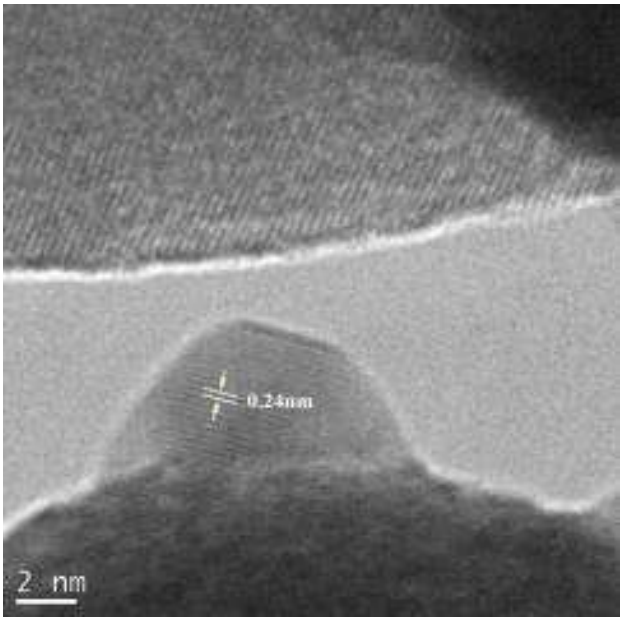

Figure S2| High-resolution image of the Ag NC under normal TEM imaging. The structure remains single-crystal and quite stable under electron beam irradiation during normal imaging.

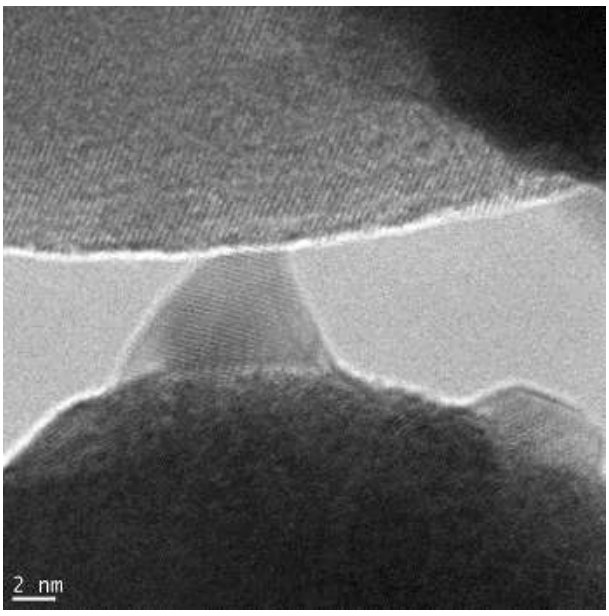

Figure S3| High-resolution image of the Ag NC during squeezing. The structure also represents single-crystal structure without any dislocations.

3. Recoverable shape evolution during compression and elongation

Please find the attached GIF file named Video S1, Video S2 and Video S3

DOI: 10.1038/NMAT4105

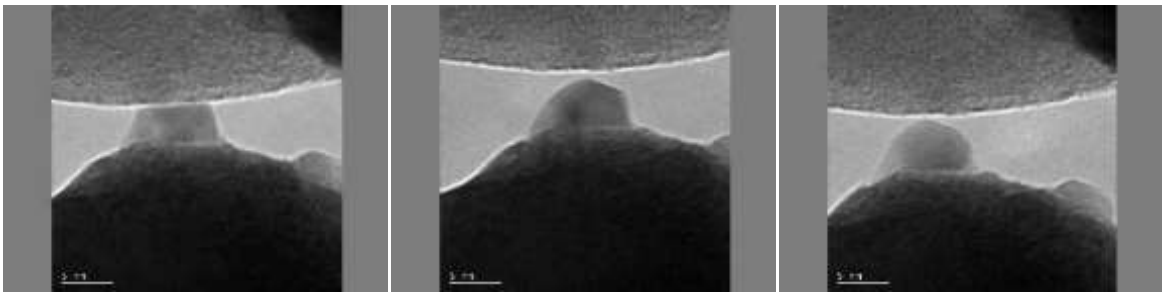

4. Splitting the Ag NC into two smaller NCs

The obtained two small nanocrystals also present superelastic properties. Please find the attached GIF file named Video S4.

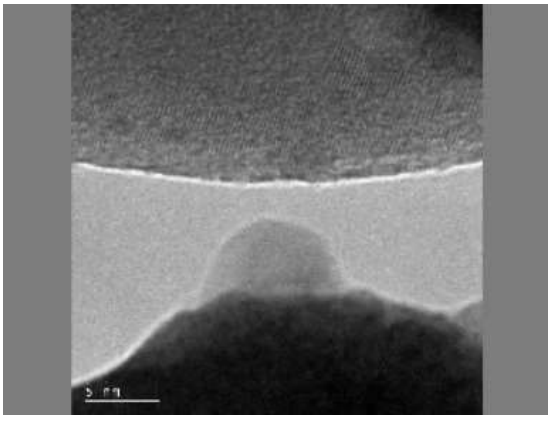

5. Surface reconstruction during deformation

Please find the movies named Video S5.wmv and Video S6.wmv

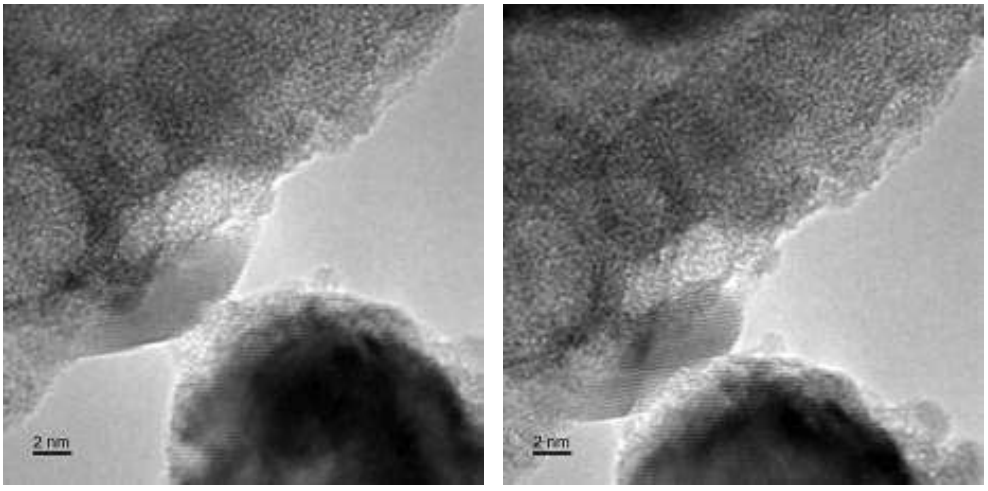

6. Shrinkage of a sharp Ag tip due to surface tension

Please find the movie named Video S7.wmv

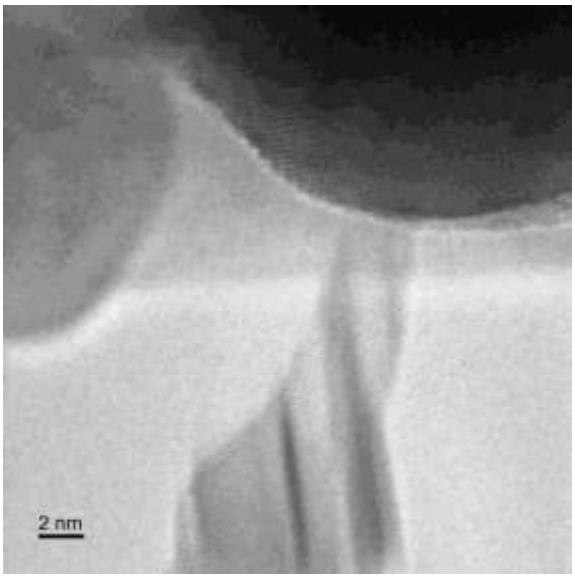

7. MD simulations of liquid-like surface diffusions for a 10 nm Ag particle at 800 K (Movie S8)

http://li.mit.edu/Stuff/YuchiehLo/Upload/Ag_800K_m1.wmv

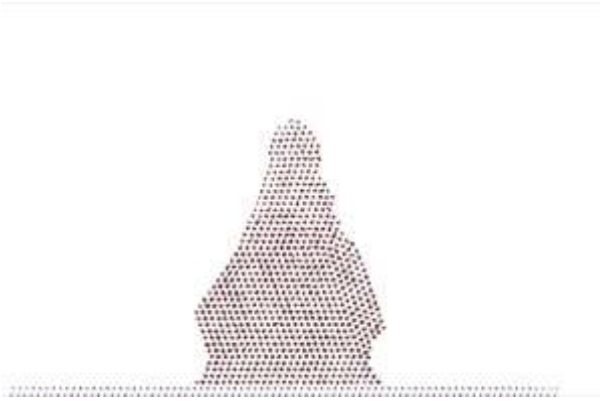

DOI: 10.1038/NMAT4105

http://li.mit.edu/Stuff/YuchiehLo/Upload/Ag_800K_m2.wmv

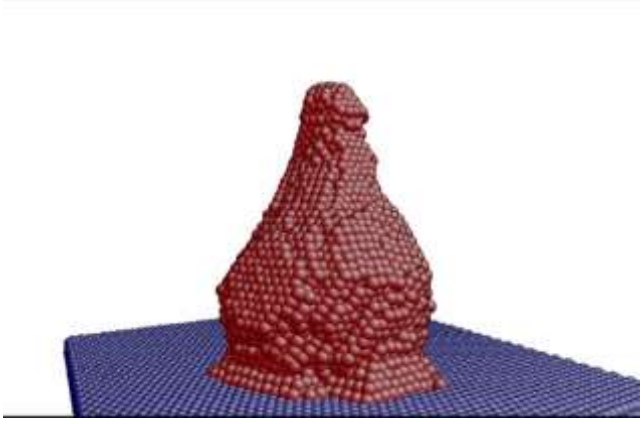

http://li.mit.edu/Stuff/YuchiehLo/Upload/Ag_800K_m3.avi

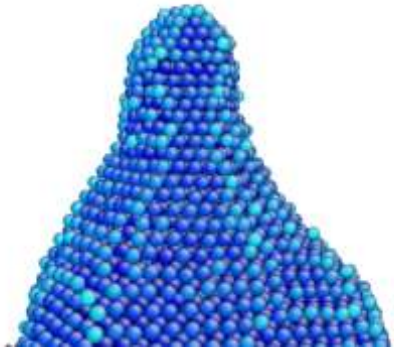

http://li.mit.edu/Stuff/YuchiehLo/Upload/Ag_800K_m4.avi

8. MD simulations of liquid-like surface diffusions for a 10 nm Ag particle at 900 K (Movie S9)

http://li.mit.edu/Stuff/YuchiehLo/Upload/Ag_900K_m1.avi

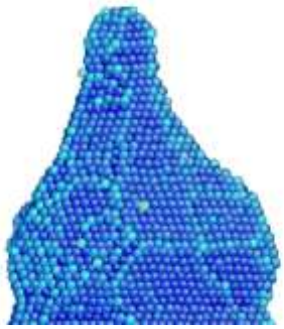

9. MD simulations of liquid-like surface diffusions for a 10 nm Ag particle at 1000 K (Movie S10)

http://li.mit.edu/Stuff/YuchiehLo/Upload/Ag_1000K_m1.avi

DOI: 10.1038/NMAT4105

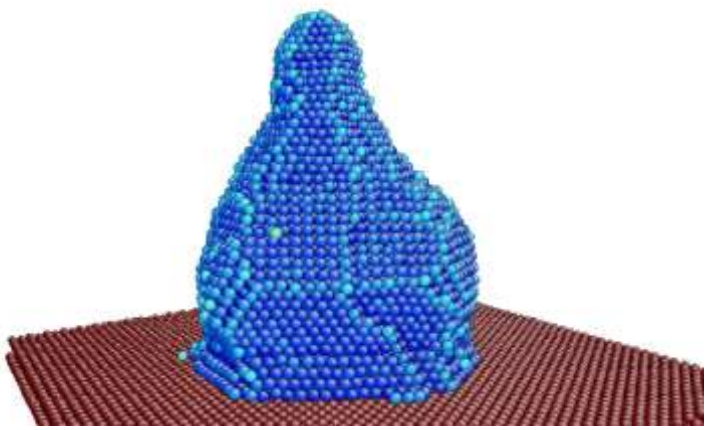

10. Illustration of curvature-driven surface diffusion

An atom in the surface layer performs random walk, but drifts with average speed $v = -M_s \partial_s \mu$.

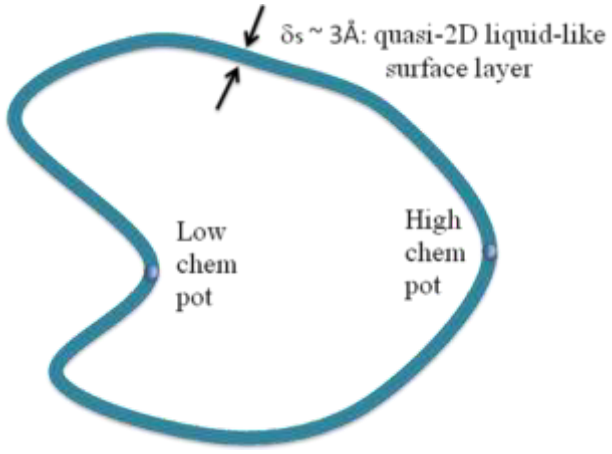

$$\mu(\mathbf{x}) = \frac{\gamma\Omega}{R(\mathbf{x})}$$

μ [J]: chemical potential

$\mathbf{x}$ [m]: position

γ [~ 1 J/m^2]: surface energy

Ω [~ 1e-29 m^3] : atomic volume

R [m] : radius of curvature

$v = -M_s \partial_s \mu$

v [m/s] : average drift speed of atom in surface layer

$-\partial_s \mu$ [J/m] : thermodynamic driving force for drift

s [m] : arc length along surface

M_s [m^2/s/J] : surface mobility

Einstein relation: $M_s = \frac{D_s}{k_B T}$

D_s [m^2/s] : surface diffusivity

$J_s = \frac{X_s}{\Omega} \delta_s v = -\frac{X_s}{\Omega} \delta_s \frac{D_s}{k_B T} \partial_s \mu$

J_s [#atoms/m/s] : number of atoms crossing surface cut per length per time

X_s [dimensionless] ≤ 1 : solubility of diffusing atom in surface liquid layer

$1/\Omega$ [$1/m^3$] : number density of atoms inside surface layer

Deposition rate: $\partial_t h + \Omega \partial_s J_s = 0$

$\partial_t h$ [m/s] : speed of surface height increase

$\partial_s J_s$ [#atoms/m^2/s] : divergence of surface flux

$\partial_t h = \frac{X_s \delta_s D_s}{k_B T} \partial_s^2 \mu = \frac{\gamma \Omega X_s \delta_s D_s}{k_B T} \partial_s^2 \frac{1}{R(s)}$

Use the final radius of curvature R_0 as an order of magnitude estimate of the magnitude of radius of curvature during the shape evolution

DOI: 10.1038/NMAT4105

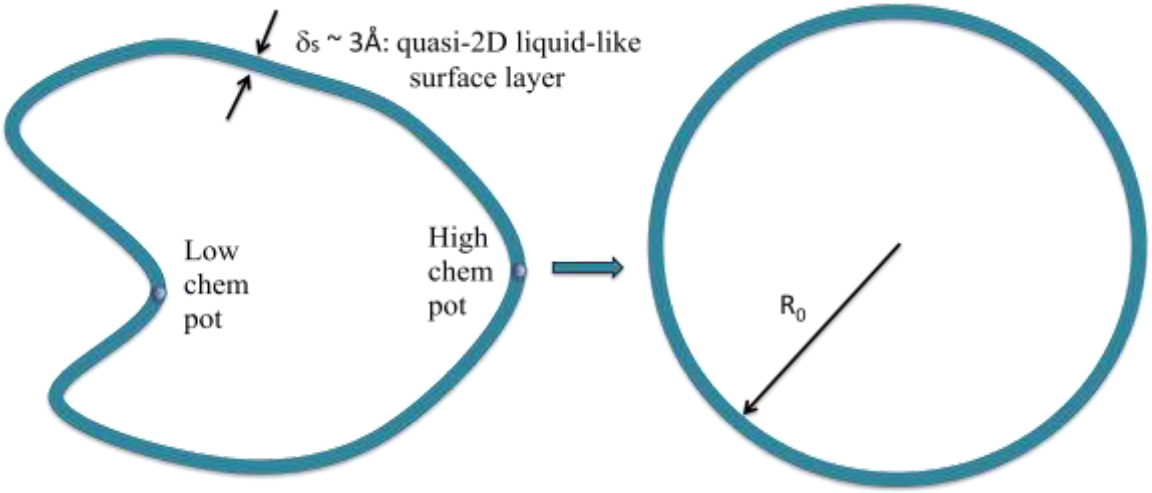

τ [s] : timescale of the shape evolution

$\partial_t h \sim \frac{R_0}{\tau}$: height change necessary to accomplish the shape change

$$\partial_s^2 \frac{1}{R(s)} \sim \frac{1}{R_0^3}$$

$$\frac{R_0}{\tau} \sim \frac{\gamma \Omega X_s \delta_s D_s}{k_B T} \frac{1}{R_0^3}$$

11. Table SI| A summary of activation energy barriers (eV) of diffusion events on Ag surfaces from Kim et al's database[21,22]

Diffusion mechanisms	(001)	$(110)_{\text{out-channel}}$	$(110)_{\text{in-channel}}$	(111)
Single atom	0.62	0.81	0.27	0.06
Two atoms	0.77	1.43	0.51	0.11
Three atoms	1.09	2.11	0.74	0.18
Four atoms	1.37	3.11	0.98	-----
Ascending adatoms	0.81	-----	0.77	0.82
Descending adatoms	0.59	-----	0.59	0.33

Leaving the corner	0.72	0.76	0.46	0.49
Approaching the corner	0.29	0.75	0.26	0.29

Table SII| Transition time (pico second) of adatom diffusions on (001) and (111) surfaces calculated by strain boost and bond boost methods[29,30]

Temperature	$t(001)_{strainboost}$	$t(001)_{bondboost}$	$t(111)_{MD}$
300 K	9.56×10^{6}	1.02×10^{7}	3.22
400 K	1.95×10^{5}	4.75×10^{4}	1.92
500 K	7.2×10^{3}	5.23×10^{3}	1.66
600 K	6.18×10^{2}	6.20×10^{2}	1.31
700 K	2.86×10^{2}	1.12×10^{2}	1.75
800 K	1.01×10^{2}	55.37	1.20
900 K	14.17	11.06	1.04
1000 K	7.57	3.93	0.74

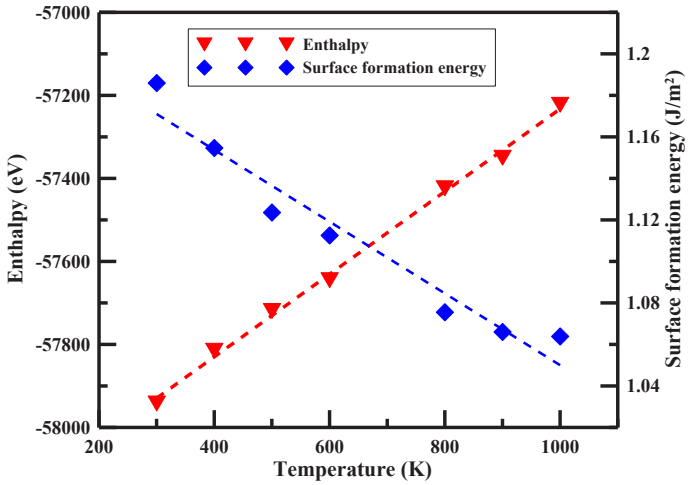

Figure S4| Enthalpy and surface formation energy of Ag particle as a function of temperature.

DOI: 10.1038/NMAT4105

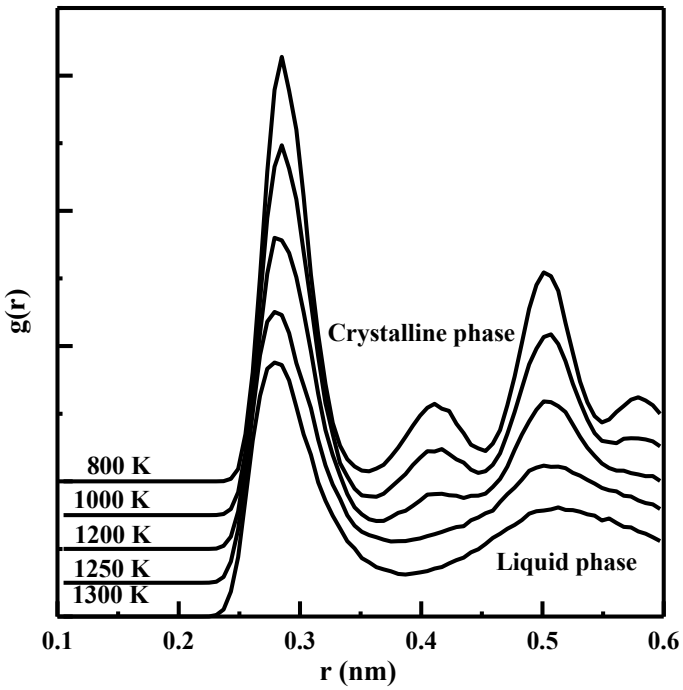

Figure S5| Radial distribution functions of Ag particle as a function of temperature.

12. The extrapolation of time scale in MD simulations

Since our MD simulations showed that the particle surface mostly consisted of (111), (001) facets, we applied accelerated MD methods to estimate the transition rates of adatom diffusion on (001) and (111) surfaces at different temperatures and listed the results in Table SII[29,30]. The average transition time of adatom diffusion on (001) and (111) surfaces at 300 K are 10 μs and 3 ps, respectively. The distribution of average transition time at different temperatures shows a straight-line behavior in the Arrhenius plot (Figure 5). The time scale of diffusion events between 300 and 800 K shows only slight difference on (111), but varies by 5~6 order for adatom diffusions on (001) surface, due to the larger activation energy. The enthalpy of 10 nm Ag particle presents a linear relationship between 300 K and 800 K (Figure S4), which implies no phase transformation during the temperature range. Therefore, most diffusion processes occurring at 800 K may be extrapolated to 300 K directly in the Arrhenius fashion. According to the data in table SII, we extrapolated the time scale of the shape-change at 300 K by t_{800K}^{MD} (MD simulation time at 800K) × $10^{5\sim6}$ (difference of time scale). Then we concluded that the approximation of shape evolution at room temperature

should be 0.01 ~ 0.1 s for the simulated geometry, which has a radius of curvature about half of that of the experiments.

Moreover, melting of the nanoparticle will occur only at the temperature above 1200 K based on the radial distribution functions of nanoparticle in Fig. S5. The tip of nanoparticle may locally melt at 1100 K before the nanoparticle changes to a semi-sphere shape. Below 1000 K the nanoparticle of 10 nm in size always stays highly crystalline. Consequently, the effect of melting can be eliminated from this work.

13. The melting point of metal NCs

One may suspect that the Ag NC might have a melting point reduced to room temperature due to size effect, and its "liquid-like" deformation behavior is the result of such size dependent melting. However, both calculations and previous experimental work[8,9,32-36] show that the melting points of Ag, Au, Al, Cu and etc. at size scale of 5 nm are still high above RT. The Ag NC here clearly shows crystal structure before and during deformation. It therefore indicates a new mechanical behavior rather than melting.

14. The beam effect on temperature

The e-beam heating effect in our experiments is not a primary factor in this liquid-like behavior of Ag nanocrystals. It is sure that surface diffusion can be influenced by electron beam irradiation. To reduce this influence, we used very weak beam intensity (around **3.8 A/cm^2**) for imaging. This beam intensity is far lower than the published literatures below.

1) D. J. Smith et al Nature (1985) 317, 5 and Science (1986) 233, 872: **20-40A/cm^2**

2) S. Iijima et al PRL (1986) 56, 6: **around 200 A/cm^2**

3) P.M. Ajayan and L.D. Marks PRL (1989) 63, 3: **10-100 A/cm^2**

4) D. Ugarte et al PRL (2000) 85, 4124: **120A/cm^2**

5) Z.W. Wang & R. E. Palmer PRL (2012) 108, 245502: **>48 A/cm^2**

In our experiments, the Ag nanocrystal maintained its structure well under this weak beam current. Atoms hopping and diffusion became activated only when the nanocrystal was under compression or relaxation after deformed. So the acceleration of surface diffusion by e-beam

DOI: 10.1038/NMAT4105

is not observed in our experiment under above conditions. We also tried to squeezing the Ag nanocrystal with e-beam blocked. The Ag nanocrystal could still recover back similar to its initial geometry, indicating that the e-beam effect should not play a critical role. As shown in Figure R1, we first took an image of the Ag nanoparticle, then we turned off the e-beam and performed the same compressing and detaching processes in the following 148 seconds. At last, we turn on the e-beam and took another image. The results showed that the Ag nanoparticle had recovered its original shape. Since the e-beam was turned off, the heating effect could also be excluded.

Theoretically, the e-beam induced temperature rise could be estimated by Fisher's model [**Radiat. Eff. (1970) 5, 239**]:

$$\Delta T = \frac{I}{4\pi k e}\left(\frac{\Delta E}{d}\right)(1 + 2\ln\frac{b}{r_0})$$

where △T is the maximum temperature rise caused by an electron beam, k is the thermal conductivity of tungsten, I is the beam current, △E is the total energy loss per electron in a sample of thickness d, b is the radius of the heat sink, and r_0 is the beam radius. The essence of Fisher's model is that the heat generation (in an incident beam of diameter d) is balanced by heat loss due to radial conduction. Because energy losses in the sample were small compared to the initial energy (200 keV), the term △E/d was equal to the stopping power of electrons, dE/dx, which was calculated from the Bethe-Bloch equation[**J. Appl. Phys. (1995) 78, 974**]:

$$-\frac{dE}{dx} = \frac{2\pi Z\rho(e^2/4\pi\varepsilon_0)^2}{m\upsilon^2}\left\{\ln\left[\frac{E(E+mc^2)^2\beta^2}{2I_e^2mc^2}\right] + (1-\beta^2) - (1-\sqrt{1-\beta^2}+\beta^2)\ln 2 + \frac{1}{8}(1-\sqrt{1-\beta^2})^2\right\}$$

where Z is the atomic number of the target element, ρ is the atomic density, ε_0 is the dielectric constant, m is the electron rest mass, ν is the electron velocity, c is the speed of light, E is the electron energy, I_e is the average excitation energy of electrons in the target, and β=ν/c. In our study, the acceleration voltage is 200 kV; thus, β=0.6946 and ν=2.0837×10^8 m/s., m=9.3×10^{-31} kg, e=1.6×10^{-19} C, ε_0=8.85×10^{-12}F/m, I=4.8 nA, b=1.5mm, and r_0=0.2 μm.

The first step is to determine the range of temperature rise of tungsten probe.

For W, Z=74, I_e=8.8×Z=651.2 eV, ρ=6.3×10^{28} m^{-3}(the mass density is 19250 kg m^{-3}), and thermal conductivity of tungsten k=173 $Wm^{-1}K^{-1}$. It is found that the maximum temperature increase of tungsten probe was estimated to be 0.079K, i.e. the tungsten could be seen at room temperature. It is an obvious discrimination compared with nanoparticle located on low thermal conductivity substrate (e.g. amorphous carbon film) [**Appl. Phys. Lett. (1987) 50, 1760**]. The second step is analyzing the temperature of silver nanoparticle. The heat injection per unit time on silver nanoparticle by electron irradiation could be summarized as:

$q = (I/e)\triangle E$, where q is the heat injection, I is the beam current on silver nanoparticle, $\triangle E$ is the average energy loss per inelastic collision [**J. Appl. Phys. (1995) 78, 974;Micron (2004) 35, 399**]. Considering that the electron energy loss in the sample is negligible compared to the initial energy, (dE/dx) can be assumed constant, so $\triangle E$ could be obtained by the following:

$$\Delta E = \frac{dE}{dx} * d,$$

Where d is the thickness of silver nanoparticle, $\frac{dE}{dx}$ could be obtained by aforementioned Bethe-Bloch equation. For Ag, Z=47, ρ=5.86×10^{28} m^{-3}(the mass density is 10490 kg m^{-3}) and I_e=8.8×Z=413.6 eV.

According to above parameter, we could found the heat injection per unit time on silver nanoparticle by electron irradiation q is 4.256×10^{-11}J/s. The injected energy q would transport heat across the interface between Ag and tungsten and induce a temperature gradient. To determine the temperature difference between the Ag nanoparticle and the W tip, the interface is taken into account. Since most phonon mediated interfaces (dielectric-dielectric and metal-dielectric) have thermal conductances between 80 and 300 $MWm^{-2}K^{-1}$ [**http://en.wikipedia.org/wiki/Interfacial_thermal_resistance**], our Ag-W interface should have a conductance in the range of 10^2 MW m^{-2} K^{-1}(considering a thin oxide layer formed). Taking into account the contacting area, the interface thermal conductance G is estimated to be 10^{-8} W/K. According to the definition of thermal resistance, $q = \Delta T * G$, the temperature difference between Ag nanoparticle and W substrate ΔT is in the range of 10^{-3} K, which is extremely small.

In conclusion, the electron beam density is 3.8 A/cm^{-2} and very small, the thermal conductivities of W substrate and W-Ag interface are high and in the range of 10^2 W/m/K. So

DOI: 10.1038/NMAT4105

the e-beam induced heating effect is not a primary factor. Also, many literatures [**J. Phys. Chem. B (2005) 109, 9703; Appl. Phys. Lett. (1987) 50, 1760**] support this conclusion that the temperature rise is very small when the electron beam density is small and the thermal conductivity is good. Williams *et al* [**Appl. Phys. Lett. (1987) 50, 1760**] have reported that the irradiation induced Au nanoparticle temperature rise occurs only at low thermal conductivity substrates.

15. The difference between "pseudoelastic" and "reversible plastic"

In this paper, the 'pseudoelastic' we mentioned is not just 'reversible plastic'. See illustration Figure S6 below for the standard definitions of pseudoelasticity and plasticity. While both pseudoelasticity and plasticity involve dissipation, and indeed most plastic strain is reversible, the latter requires imposing a negative load, while the former returns completely at still positive load. This is fundamental, because pseudoelastic deformation cannot have plastic strain ("locked in" even at zero stress). And plastic strain is of course what makes plastic forming possible.

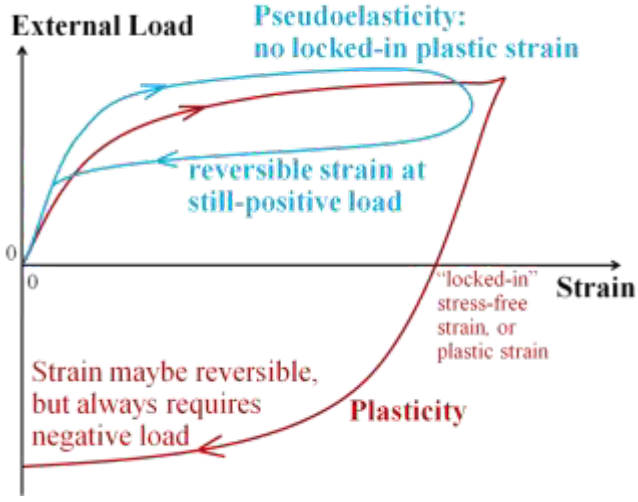

Figure S6. Illustration of pseudoelastic deformation and reversible plastic deformation.

During compression, the Ag nanoparticle deforms plastically due to W tip squeezing. However, during detaching, the shape recover is driven by surface energy. The Vander Waals force isn't the driving force.

16. Laterally squeezing a Ag nanoparticle show perfect recovery from its deformed form

Sometimes, laterally squeezing a Ag nanoparticle can show the possibility of perfect recovery of the deformed form, as shown in Figure S7. The Ag nanoparticle demonstrates the exactly same height of 41 atomic layers and same top size of 2.4 nm before (Figure S7a) and after (Figure S7h) compression.

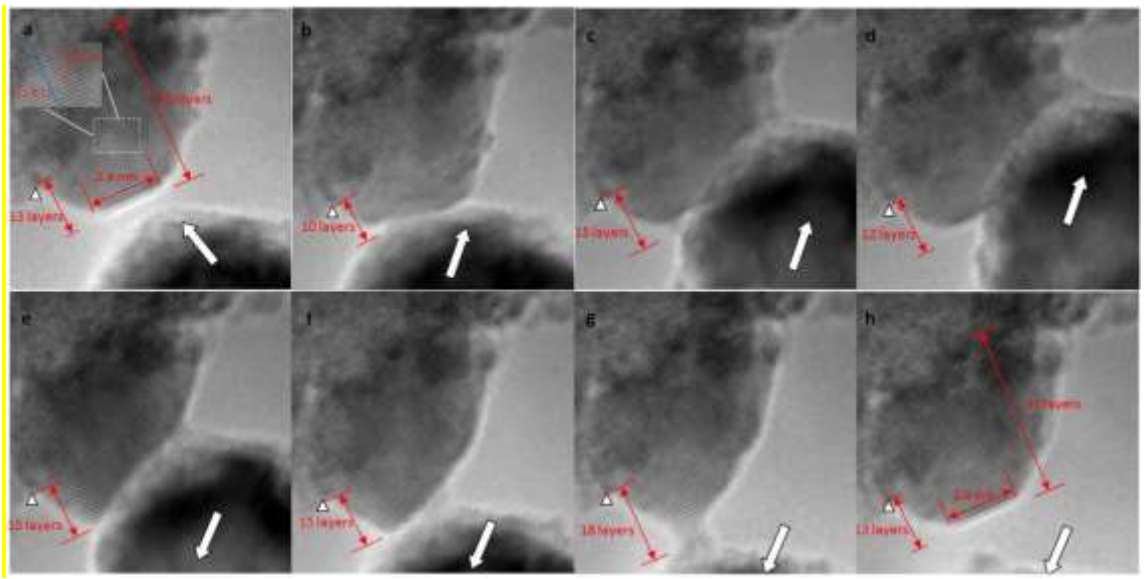

Figure S7. An image sequence of squeezing a sub-10nm sized Ag nanoparticle. The white triangle is an anchor point. The white arrow shows the moving direction of the W tip (bottom).